

The rise and fall of a challenger: the Bullet Cluster in Λ cold dark matter simulations

Robert Thompson^{1,2}, Romeel Davé^{1,3,4}, Kentaro Nagamine^{5,6}

¹ *University of the Western Cape, Bellville, Cape Town 7535, South Africa*

² *Astronomy Department, University of Arizona, Tucson, AZ 85721, USA*

³ *South African Astronomical Observatory, Observatory, Cape Town 7925, South Africa*

⁴ *African Institute for Mathematical Sciences, Muizenberg, Cape Town 7945, South Africa*

⁵ *Department of Earth and Space Science, Graduate School of Science, Osaka University, 1-1 Machikaneyama-cho, Toyonaka, Osaka 560-0043, Japan*

⁶ *Department of Physics and Astronomy, University of Nevada, Las Vegas, 4505 S. Maryland Pkwy, Las Vegas, NV 89154-4002, USA*

30 June 2015

ABSTRACT

The Bullet Cluster has provided some of the best evidence for the Λ cold dark matter (ACDM) model via direct empirical proof of the existence of collisionless dark matter, while posing a serious challenge owing to the unusually high inferred pairwise velocities of its progenitor clusters. Here we investigate the probability of finding such a high-velocity pair in large-volume N-body simulations, particularly focusing on differences between halo finding algorithms. We find that algorithms that do not account for the kinematics of infalling groups yield vastly different statistics and probabilities. When employing the ROCKSTAR halo finder that considers particle velocities, we find numerous Bullet-like pair candidates that closely match not only the high pairwise velocity, but also the mass, mass ratio, separation distance, and collision angle of the initial conditions that have been shown to produce the Bullet Cluster in non-cosmological hydrodynamic simulations. The probability of finding a high pairwise velocity pair among haloes with $M_{\text{halo}} \geq 10^{14} M_{\odot}$ is 4.6×10^{-4} using ROCKSTAR, while it is $\approx 34\times$ lower using a friends-of-friends (FOF) based approach as in previous studies. This is because the typical spatial extent of Bullet progenitors is such that FOF tends to group them into a single halo despite clearly distinct kinematics. Further requiring an appropriately high average mass among the two progenitors, we find the comoving number density of potential Bullet-like candidates to be on the order of $\approx 10^{-10} \text{ Mpc}^{-3}$. Our findings suggest that Λ CDM straightforwardly produces massive, high relative velocity halo pairs analogous to Bullet Cluster progenitors, and hence the Bullet Cluster does not present a challenge to the Λ CDM model.

Key words: method : N-body simulations — galaxies : evolution — galaxies : formation — galaxies: clusters — cosmology : theory — cosmology : dark matter

1 INTRODUCTION

Observations of merging massive clusters such as the Bullet Cluster (1E0657-56) provide a unique opportunity to test the Λ CDM paradigm. This particular object consists of two massive clusters that have recently passed through one another and are separated by $\simeq 0.72 \text{ Mpc}$ on the sky at an observed redshift of $z = 0.296$ (Clowe et al. 2004, 2006; Bradač et al. 2006). This system is relatively unique due to the collision trajectory being almost perpendicular to our line of sight. Both clusters are also quite massive and hence rare, with $M_{\text{parent}} \simeq 1.5 \times 10^{15} M_{\odot}$ & $M_{\text{bullet}} \simeq 1.5 \times 10^{14} M_{\odot}$ (Clowe et al. 2004, 2006; Bradač et al. 2006). *Chandra* X-ray observations revealed that the primary baryonic component

has been stripped away from the primary mass component (identified via weak lensing) in the collision, and resides between the two massive clusters in the form of hot X-ray emitting gas (Markevitch 2006). This evidence provided direct empirical proof for the existence of collisionless and mass-dominant dark matter (Clowe et al. 2006).

Shock features in the gas have been used to infer the velocity of the bow shock preceding the ‘bullet’ ($v_{\text{shock}} = 4740^{+710}_{-550} \text{ km s}^{-1}$; Markevitch 2006), which was initially assumed to be approximately the infall velocity of the ‘bullet’ itself. Through the use of non-cosmological hydrodynamic simulations, several groups have shown that this is not necessarily the case (Milosavljević et al. 2007; Springel & Farrar 2007; Mastropietro & Burkert 2008; Lage & Farrar 2014b).

Halo pair (indicated by the subscript ‘12’) initial configurations varied with separation distances (d_{12}) ranging from $\sim 3.4\text{--}5\text{ Mpc}$, M_{parent} (M_1) from $7.13 \times 10^{14} \text{--} 1.91 \times 10^{15} M_{\odot}$, M_{bullet} (M_2) from $1.14 \times 10^{14} \text{--} 2.59 \times 10^{14} M_{\odot}$, and pairwise velocities (v_{12}) ranging from $2057 \text{--} 3980 \text{ km s}^{-1}$ at $z \simeq 0.5$. Mastropietro & Burkert (2008) in particular, set the initial halo requirements to be $M_1 \simeq 7.13 \times 10^{14} M_{\odot}$, $M_2 \simeq 1.14 \times 10^{14} M_{\odot}$, and $v_{12} \simeq 3000 \text{ km s}^{-1}$ at a separation distance of $d_{12} \simeq 5 \text{ Mpc}$. More recent work by Lage & Farrar (2014a) has revised these values to $M_1 \simeq 1.91 \times 10^{15} M_{\odot}$, $M_2 \simeq 2.59 \times 10^{14} M_{\odot}$, and $v_{12} \simeq 2799 \text{ km s}^{-1}$ at a separation distance of $d_{12} \simeq 2.8 \text{ Mpc}$.

Reproducing such a massive, close, and high- v_{12} merging pair in large N-body cosmological simulations has proven to be very challenging (Hayashi & White 2006; Lee & Komatsu 2010; Thompson & Nagamine 2012; Watson et al. 2014; Bouillot et al. 2014), potentially suggesting that the canonical ΛCDM model with Gaussian perturbations is inconsistent with the observed Bullet Cluster. Improving upon the work of Lee & Komatsu (2010), Thompson & Nagamine (2012) calculated the probability of finding a halo pair with $v_{12} \geq 3000 \text{ km s}^{-1}$ among all halo pairs with $M_1, M_2 \geq 10^{14} M_{\odot}$ and $d_{12} \leq 10 \text{ Mpc}$ to be $P = 2.8 \times 10^{-8}$. Extrapolating their cumulative v_{12} curve, they estimated that one would need a box size of at least $\simeq (6.25 \text{ Gpc})^3$ to produce one Bullet-like pair.

Bouillot et al. (2014) argue that the simulations of Lee & Komatsu (2010) and Thompson & Nagamine (2012) were too limited in volume ($(4.3 \text{ Gpc})^3$ and $(2.8 \text{ Gpc})^3$ respectively) to properly characterise the tail of the v_{12} distribution. They estimated the probability of finding a Bullet-like cluster in a $(29 \text{ Gpc})^3$ simulation to be $P(v_{12} > 3000 \text{ km s}^{-1}) = 6.4 \times 10^{-6}$, which is two orders of magnitude larger than estimates by Thompson & Nagamine (2012). However, even with an improved probability in such a large volume, Bouillot et al. (2014) did not find any halo pairs matching the initial configurations required to reproduce the observed properties of 1E0657-56 (Mastropietro & Burkert 2008; Lage & Farrar 2014a).

The simulations analysed by Lee & Komatsu (2010), Thompson & Nagamine (2012), and Bouillot et al. (2014) have one crucial aspect in common: each group used a variant of the friends-of-friends (FOF) algorithm (e.g., Davis et al. 1985) to identify and group their dark matter particles into haloes. It is known that FOF tends to ‘over-group’ the dark matter haloes when the resolution of the simulation is not adequate. It is often the case that a trace amount of particles bridge the two haloes, resulting in them being identified as a single dumbbell-shaped group. When the overlap between the two haloes is more significant, FOF has no way of separating them into two components.

In this paper, we demonstrate that in the context of searching for a close, massive, high- v_{12} pair, one cannot accurately identify haloes based solely on the spatial distribution of particles, as FOF does. To properly separate and identify substructures, we must also consider the particle velocities. The recently developed ROCKSTAR halo finder (Behroozi et al. 2013) provides a way to do so. We use ROCKSTAR to calculate more robust statistics and probabilities for finding close, massive, high- v_{12} halo pairs in a large cosmological N-body simulation. We find much greater numbers of such pairs than in previous works, and moreover

Table 1. Simulations

Run Name	Box Size [Mpc]	Particle Count	M_{dm} [M_{\odot}]	ϵ [kpc]
L6249	6429	1600^3	2.64×10^{12}	160.7
L3214	3214	800^3	2.64×10^{12}	160.7
L1607	1607	400^3	2.64×10^{12}	160.7

Note. — Summary of simulations used in this paper. M_{dm} is the mass of each dark matter particle, and ϵ is the comoving gravitational softening length. We have incorporated the effect of the Hubble parameter ‘ h ’ in the numbers shown in the table and throughout this paper.

they reasonably match the required initial configurations of Mastropietro & Burkert (2008) and Lage & Farrar (2014a) in mass, mass ratio, d_{12} , collision angle, and v_{12} .

This paper is organized as follows: in Section 2 we detail our simulations. Section 3 details the halo finding algorithms. We present our results in Section 4. Section 5 contains concluding remarks and discussion.

2 SIMULATIONS

For our simulations we use the GADGET-3 code (Springel 2005), which simulates large N-body systems by means of calculating gravitational interactions with a hierarchical multipole expansion. It uses a particle-mesh method for long-range forces and a tree method for short-range forces.

Initial conditions are initialized at $z = 99$ using N-GenIC¹. We assume cosmological parameters consistent with constraints from the WMAP (Hinshaw et al. 2013) & Planck (Planck Collaboration et al. 2013) results, namely $\Omega_m = 0.3$, $\Omega_{\Lambda} = 0.7$, $H_0 = 70$, $\sigma_8 = 0.8$, $n_s = 0.96$. Our largest simulation employs 1600^3 collision-less dark matter (DM) particles in a $(6.4 \text{ Gpc})^3$ volume with an effective force resolution of $\epsilon = 160.7 \text{ kpc}$ (i.e., comoving gravitational softening length). Two simulations with smaller volumes $((3.2 \text{ Gpc})^3$ and $(1.6 \text{ Gpc})^3$) and particle counts (800^3 and 400^3) were ran with the same force resolution to test how the simulation volume affects our results. A summary of the simulations used in this study can be found in Table 1.

3 HALO FINDERS

Identifying dark matter haloes as groups of particles within simulation data is a challenging affair, and there are numerous codes with different feature sets employing different algorithms. Knebe et al. (2011) compared a number of halo finders in both cosmological and idealized scenarios. Overall, they found most to be in agreement with one another, with only subtle variations among the results. But in detail and for specific types of systems, the differences can be substantial. Here we employ two popular group finding algorithms to

¹ <http://www.mpa-garching.mpg.de/gadget/>

group dark matter particles into haloes: a friends-of-friends algorithm, and a six-dimensional phase-space halo finder.

The FOF algorithm used in this study is a simplified version of the parallel friends-of-friends group finder SUBFIND (Springel et al. 2001) with the post-processing SUBFIND algorithm disabled. The code groups the particles into DM haloes if their positions lie within a specified linking length. This linking length is a fraction of the initial mean inter-particle separation, for which we adopt a standard value of $b = 0.15$ (More et al. 2011). Additional groupings with $b = 0.20$ were performed, whose results are briefly discussed in Section 4.3.

We also use a six-dimensional phase-space algorithm called ROCKSTAR (hereafter RS; Behroozi et al. 2013), which is based on an adaptive hierarchical refinement of friends-of-friends groups in both positional and velocity space. RS initially divides the simulation into 3D friends-of-friends groups using a $b = 0.28$. The velocity and positions of each halo are then normalized by the group position and velocity dispersions, which gives rise to a natural phase-space metric. Next, a phase-space linking length is adaptively chosen such that 70% of the group's particles are linked together in subgroups; the normalization process is then repeated for each subgroup. Once all levels of substructure are found, seed haloes are placed at the lowest substructure levels and particles are assigned hierarchically to the closest seed halo in phase space. Finally, unbound particles are removed from the group. This allows RS to more accurately identify substructure while maintaining accurate recovery of halo properties (see Knebe et al. 2011, for further details).

For most situations, FOF determines halo properties to 10% accuracy (Knebe et al. 2011). The algorithm however, is not without weaknesses. In major mergers or when subhaloes lie close to the centers of their host haloes, the density contrast is not strong enough to distinguish which particles belong to which halo. If the two haloes have some relative motion, six-dimensional halo finders (such as RS) can additionally use particle velocity information to determine halo membership (Behroozi et al. 2013).

4 RESULTS

To search for Bullet Cluster-like halo pair progenitors, we examine our simulations at $z = 0.489$ to identify systems with the required initial configurations of both Mastropietro & Burkert (2008, hereafter MB08) and Lage & Farrar (2014a, hereafter LF14).

4.1 Halo Mass Function

To check the validity of our DM halo identification, we examine the DM halo mass function in Figure 1. The mass functions of the two halo finders match remarkably well. This agreement is not surprising, because the virial masses calculated by RS include all substructure and should be comparable to the FOF halo masses. We truncate the FOF halo mass function at 32 particles, but we show the RS mass function below this in order to visualize the level of incompleteness owing to poor numerical resolution at low halo masses; we will only be concerned with haloes $\geq 10^{14} M_\odot$, above which the mass function is not limited by our resolution, and in this

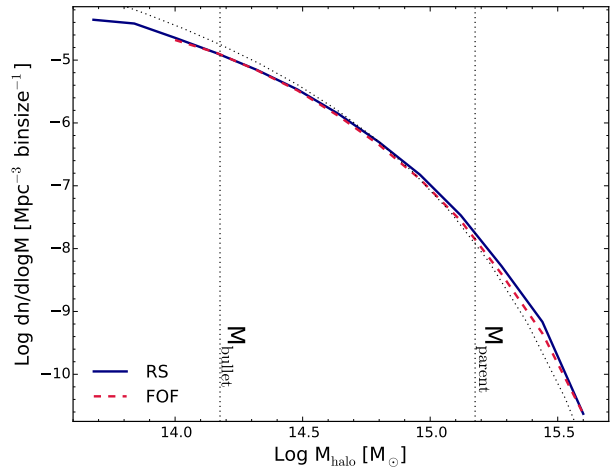


Figure 1. DM halo mass function at $z = 0.489$ for RS & FOF groupings. The vertical black dotted lines represent the mass of the observed bullet and parent respectively (Clowe et al. 2004, 2006; Bradač et al. 2006). The dashed line represents the theoretical DM halo mass function from Sheth & Tormen (1999).

regime there is little difference in the mass function between the two codes.

The black dashed line in Figure 1 is the Sheth & Tormen (1999) DM halo mass function at $z = 0.489$. Our simulations with both groupings slightly underpredict with regards to analytic theory at the low-mass end, and slightly over predict at the high-mass end. Many studies have shown that theoretical models such as Sheth & Tormen (1999) do not always agree with simulations since they do not capture the entire complexity of halo formation (i.e. Jenkins et al. 2001; Tinker et al. 2008; Robertson et al. 2009; Courtin et al. 2011). The important point here however, is that both halo identification codes agree well with each other at $M_{\text{halo}} \geq 1 \times 10^{14} M_\odot$, which corresponds to a halo with approximately 40 DM particles.

4.2 Average pair mass and pairwise velocities

We calculate pairwise velocities ($v_{12} = |\vec{v}_1 - \vec{v}_2|$) for all halo pairs with $d_{12} \leq 10$ Mpc. To examine how v_{12} relates to the mass of the halo pair, we plot the average halo pair mass ($\langle M_{12} \rangle \equiv (M_1 + M_2)/2$) as a function of v_{12} in Figure 2, for RS & FOF groupings in all three box sizes. RS clearly has a broader distribution along v_{12} in every case, a direct result of the code identifying more velocity-space substructure.

The dotted line denotes the average observed mass of the two components of the Bullet Cluster ($\langle M_{12} \rangle = 8.25 \times 10^{14} M_\odot$; Clowe et al. 2004, 2006; Bradač et al. 2006), dot-dashed lines represent the average mass and pairwise velocities of the initial condition requirements of MB08 ($\langle M_{12} \rangle = 4.14 \times 10^{14} M_\odot$ & $v_{12} \simeq 3000 \text{ km s}^{-1}$), and dashed lines are the initial condition requirements of LF14 ($\langle M_{12} \rangle = 1.08 \times 10^{15} M_\odot$ & $v_{12} \simeq 2799 \text{ km s}^{-1}$). We note that, in our larger volumes, RS identifies numerous potential Bullet progenitor candidates (in and around the upper right quadrant of each panel), whereas FOF identifies none.

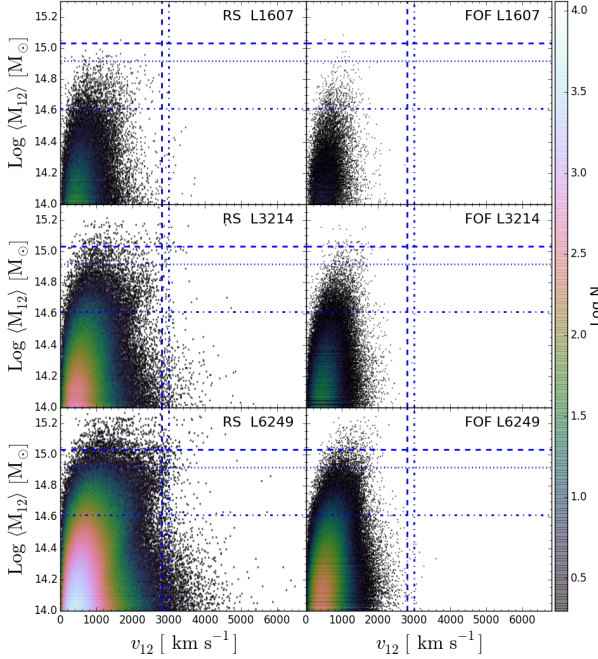


Figure 2. Average halo pair mass $\langle M_{12} \rangle$ as a function of halo pairwise velocity v_{12} . Color corresponds to the logarithmic number of data points ($\text{Log } N$). The horizontal dotted line represents the observed $\langle M_{12} \rangle$ of the Bullet Cluster ($\langle M_{12} \rangle = 8.25 \times 10^{14} M_{\odot}$; Clowe et al. 2004, 2006; Bradač et al. 2006). The dot-dashed lines represent $\langle M_{12} \rangle$ and v_{12} for the initial condition requirements of Mastropietro & Burkert (2008), while the dashed lines represent the initial requirements of Lage & Farrar (2014a).

4.3 Pairwise velocity probability distribution function

To estimate the probability of finding a Bullet Cluster candidate, the approach taken in previous works (Lee & Komatsu 2010; Thompson & Nagamine 2012; Bouillot et al. 2014) is to identify halo pairs with high relative velocities ($v_{12} \geq 3000 \text{ km s}^{-1}$; MB08) from among all halo pairs above a given mass threshold ($M_1, M_2 \geq 10^{14} M_{\odot}$) and separated by $d_{12} \leq 10 \text{ Mpc}$. The Bullet Cluster, however, has a considerably higher mass, with the main cluster having an observed mass in excess of $10^{15} M_{\odot}$ (Clowe et al. 2004, 2006; Bradač et al. 2006). Given that the usual criteria may not select pairs with mass ratios similar to the Bullet-Cluster, we refer to pairs with $M_1, M_2 \geq 10^{14} M_{\odot}$ as *high- v_{12}* pairs. To more accurately sample potential Bullet-like candidates of higher mass, we additionally restrict our sample to pairs whose average mass is greater than $4.14 \times 10^{14} M_{\odot}$ (MB08), or $1.08 \times 10^{15} M_{\odot}$ (LF14) and refer to this sample as *massive, high- v_{12}* pairs. In this section we discuss the general pairwise velocity probability distribution function (PDF) of both *high- v_{12}* and *massive, high- v_{12}* pairs before discussing the number density of these objects in the following section.

Previous works have determined the probability of finding a *high- v_{12}* pair to be on the order of $P(\geq 3000 \text{ km s}^{-1}) \simeq 10^{-8} - 10^{-9}$ (Lee & Komatsu 2010; Thompson & Nagamine

2012). Recently Bouillot et al. (2014) argued for a value two orders of magnitude larger ($P \simeq 10^{-6}$) through the examination of a simulation with a much larger volume $(29 \text{ Gpc})^3$. As we show in Section 4.2 however, identifying haloes with an FOF algorithm can lead to substantially lower values of v_{12} (Figure 2) due to its inability to distinguish between substructure in merging systems like the Bullet. These lower values of v_{12} will have a direct impact on the resulting probabilities.

Figure 3 shows the PDF and fit from our largest simulation for both RS & FOF groupings of *high- v_{12}* ($M_1, M_2 \geq 10^{14} M_{\odot}, d_{12} \leq 10 \text{ Mpc}$) pairs. The overall distribution is Gaussian-like, with a peak at $v_{12} \approx 600 \text{ km s}^{-1}$. This is comparable to the Hubble velocity for haloes separated by 6.5 Mpc. The *high- v_{12}* pairs in this sample lie in the extreme tail of the distribution at $v_{12} \geq 3000 \text{ km s}^{-1}$. Hence such high velocities are only likely to arise in systems that are merging towards each other.

The probability for a *high- v_{12}* pair is the area under this curve above the velocity threshold, divided by the total area under the curve. Because this high pairwise velocity tail is sampled by a small number of haloes owing to the limited simulation volume, it may not be a fair representation of the true statistics to simply count pairs above this threshold. One approach to mitigate this is to fit the PDF with an analytic function and integrate this function out to infinity. Previous works have used a Gaussian for this purpose (Lee & Komatsu 2010; Thompson & Nagamine 2012), but Bouillot et al. (2014) argues for the use of “Extreme Value Statistics” (EVS; Frechet 1927; Fisher & Tippett 1928; Gumbel 1935; Gnedenko 1943) since the extreme tail of the PDF can deviate significantly from a Gaussian.

Here we instead follow the approach of fitting a skewed Gaussian, but we force the fit to be very good particularly for the PDF above 3000 km s^{-1} . This is accomplished by allowing large fitting errors at $v_{12} < 3000 \text{ km s}^{-1}$, and small ones at $v_{12} \geq 3000 \text{ km s}^{-1}$. A least-square-fit then obtains a very good fit at high velocities, at the expense of a poorer fit at lower velocities. However, we do not need to use the fit at lower velocities, since there we can directly count pairs within a large and representative sample. We then calculate the probability of finding a *high- v_{12}* pair with desired statistics by integrating our best-fit skewed Gaussian to infinity.

We also show the skewed Gaussian fits (dashed lines) in Figure 3. At $v_{12} < 3000 \text{ km s}^{-1}$ the fit is not good, but as shown by the inset in the upper left, the fit is much better at $v_{12} \geq 3000 \text{ km s}^{-1}$. By integrating the fitting function from 3000 km s^{-1} to infinity we obtain probabilities of $P_{\text{RS}} = 4.58 \times 10^{-4}$ & $P_{\text{FOF}} = 1.35 \times 10^{-5}$. Again, this is the probability of finding a halo pair with $v_{12} \geq 3000 \text{ km s}^{-1}$ among all halo pairs with $d_{12} \leq 10 \text{ Mpc}$ and $M_1, M_2 \geq 10^{14} M_{\odot}$ at $z = 0.489$.

Our P_{FOF} is slightly larger than the value calculated by Bouillot et al. (2014) which may be due to our simplified approach. If we run the same analysis on FOF groupings with $b = 0.20$ as opposed to $b = 0.15$, we find $P_{\text{FOF}, b=0.20} = 3.51 \times 10^{-6}$, which is slightly smaller than the value of $P = 6.4 \times 10^{-6}$ that Bouillot et al. (2014) obtained using $b = 0.15$ for their FOF groupings. Regardless of this difference, P_{RS} remains almost two orders of magnitude higher than previous estimates using FOF.

Repeating the same exercise on the smaller boxes re-

sults in similar probabilities. For the L3214 run, we find $P_{\text{RS}} = 5.64 \times 10^{-4}$ and $P_{\text{FOF}} = 4.48 \times 10^{-6}$. And $P_{\text{RS}} = 2.46 \times 10^{-4}$ and $P_{\text{FOF}} = 3.37 \times 10^{-6}$ for the L1607 run. Note that the distribution gets noisier with decreasing box size, hence the probabilities become more unreliable. Even so, the probabilities remain roughly similar in order of magnitude, showing that this approach is stable against reasonable box size variations.

If we instead employ EVS and fit a Generalized Pareto distribution (GPD) of the form

$$\text{PDF} = \frac{1}{\sigma} \left(1 + \xi \frac{v_{12} - \mu}{\sigma} \right)^{1/\xi+1}, \quad (1)$$

as was done in Bouillot et al. (2014), we find that the probabilities do not differ drastically from our above described method. We select the location parameter (μ) in the same fashion as Bouillot et al. (2014) ($\mu = 1600 \text{ km s}^{-1}$; see their Figure 10)² before fitting for the scale (σ) and shape (ξ) parameters. These fits are shown in Figure 4 for our largest simulation as the dashed lines. Integrating these from 3000 km s^{-1} to infinity we find $P_{\text{RS,GPD}} = 4.51 \times 10^{-4}$ and $P_{\text{FOF,GPD}} = 9.31 \times 10^{-6}$, which are different by a factor of 1.02 and 1.45 when compared to our skewed normal fits. These minor differences indicate that our method is sufficient at fitting the high- v_{12} tail of the distribution.

In Figure 5, we show the ratio between the RS and FOF PDFs in our three simulation volumes using the skewed normal fits. The PDFs are very similar for $v_{12} \lesssim 1000 \text{ km s}^{-1}$, but above this value the RS probability increases markedly relative to FOF, such that by $v_{12} \sim 3000 \text{ km s}^{-1}$ it is two orders of magnitude higher. The ratio of RS & FOF PDFs in the L3214 and L1607 runs have the same trend as the L6249 run, suggesting that the statistical relation between massive RS & FOF velocity pairs does not vary drastically even in volumes as small as $(1607 \text{ Mpc})^3$.

Using the methods described above, we impose an additional mass criteria of $\langle M_{12} \rangle \geq 4.14 \times 10^{14} M_{\odot}$ (MB08) and calculate the probability of finding a *massive, high- v_{12}* halo pair within our largest volume to be $P_{\text{RS,Bullet-like}} = 1.36 \times 10^{-3}$ and $P_{\text{FOF,Bullet-like}} = 7.38 \times 10^{-6}$. Note that with the additional mass cuts we are sampling a different population of halo pairs. This results in a value of $P_{\text{RS,Bullet-like}}$ that is $\approx 3\times$ larger than P_{RS} , while $P_{\text{FOF,Bullet-like}}$ is $\approx 2\times$ smaller than P_{FOF} , indicating that a greater fraction of $\langle M_{12} \rangle \geq 4.14 \times 10^{14} M_{\odot}$ halo pairs within the RS groupings have a v_{12} greater than 3000 km s^{-1} . Nonetheless, we will show in the next section that such *massive, high- v_{12}* pairs are globally less frequent than *high- v_{12}* pairs by an order of magnitude.

We note that for the above quoted statistics we are imposing the velocity requirement of $v_{12} \geq 3000 \text{ km s}^{-1}$ from MB08 in order to compare to previous works. If we instead use the velocity requirement of $v_{12} \geq 2799 \text{ km s}^{-1}$ argued by LF14 we find $P_{\text{RS}}(\geq 2799 \text{ km s}^{-1}) = 7.57 \times 10^{-4}$ and $P_{\text{FOF}}(\geq 2799 \text{ km s}^{-1}) = 2.89 \times 10^{-5}$ amongst all halos with $M_1, M_2 \geq 10^{14} M_{\odot}$. Imposing the additional mass cut of $\langle M_{12} \rangle \geq 1.08 \times 10^{15} M_{\odot}$ (LF14) we find $P_{\text{RS,Bullet-like}}(\geq 2799 \text{ km s}^{-1}) = 5.84 \times 10^{-2}$ and

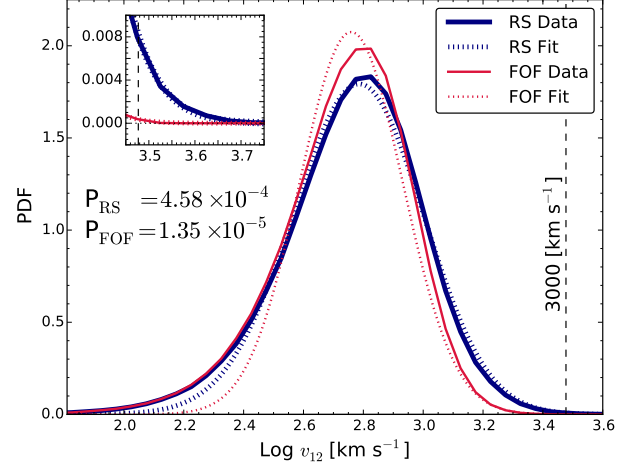


Figure 3. Probability distribution function of massive halo pairs ($M_1, M_2 \geq 10^{14} M_{\odot}, d_{12} \leq 10 \text{ Mpc}$) in our largest simulation (L6249) identified by FOF and RS. Thin red solid line represents the FOF data and the thick blue solid line shows RS. Dashed lines represent the skew normal fit to the data. Small error bars were applied at $v_{12} \geq 3000 \text{ km s}^{-1}$ (MB08) to force the fit to be better there, at the expense of a poor fit at lower v_{12} . Inset shows the fit at $v_{12} \geq 3000 \text{ km s}^{-1}$, demonstrating the excellent fit in the high velocity tail. We also show the probability of finding a halo pair with $v_{12} \geq 3000 \text{ km s}^{-1}$ obtained by integrating the fitting functions to ∞ .

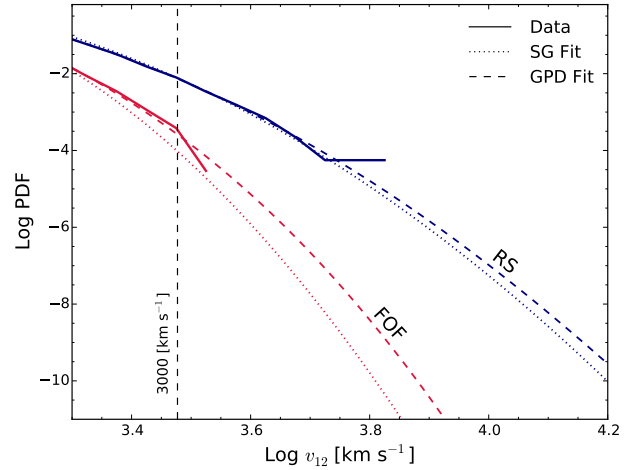


Figure 4. Figure 3 plotted in log-log space, zoomed in on the high pairwise velocity tail. The skewed normal fits (SG; described in Section 4.3) are plotted as the dotted lines, while the Generalized Pareto distributions (GPD) are shown as the dashed lines.

$P_{\text{FOF,Bullet-like}}(\geq 2799 \text{ km s}^{-1}) = 9.41 \times 10^{-6}$. A summary of these probabilities can be found in Table 2.

4.4 Number density estimation

In order to quantify whether these objects are a likely occurrence in Λ CDM, we must estimate their number densities. This will also provide predictions for future all-sky surveys

² We note that the exact value of μ has a minimal impact on the resulting probabilities

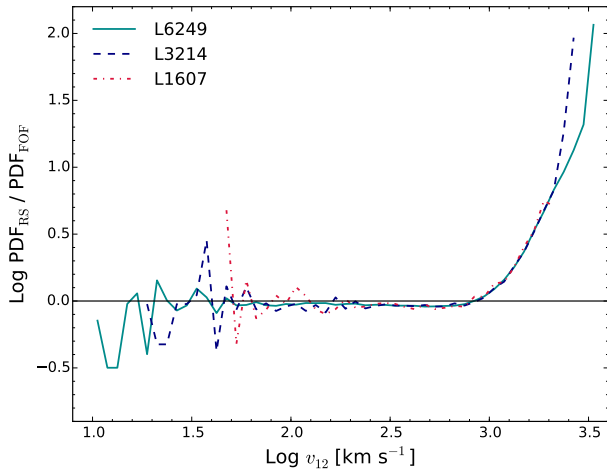


Figure 5. Ratio between FOF & RS PDFs, for all three simulation box sizes. The two halo finders agree well up to $v_{12} \sim 1000 \text{ km s}^{-1}$, but RS rapidly increases relative to FOF above this. The PDF are consistent among the various box sizes.

that may be able to probe deeper and hence see such objects over a larger volume.

In our largest volume simulation, the number of halo pairs with $d_{12} \leq 10 \text{ Mpc}$, $M_1, M_2 \geq 10^{14} M_\odot$, and $v_{12} \geq 3000 \text{ km s}^{-1}$ (MB08) is 6 using FOF and 318 using RS. To obtain the full number density, we must additionally correct for our finite volume. Using the integrated PDF (P) described in previous sections, the number of halo pairs within our sample above the v_{12} threshold ($N(\geq v_{th})$), and the total number of halo pairs within our sample (N ; Section 4.3) we calculate the correction factor to be

$$n_{\text{correction}} = \frac{P}{N(\geq v_{th})/N}. \quad (2)$$

This results in an additional factor of 1.03 for RS and 1.53 for FOF. Dividing by our simulation volume, we thus obtain the values of $n_{\text{RS}} = 1.23 \times 10^{-9} \text{ Mpc}^{-3}$ and $n_{\text{FOF}} = 3.45 \times 10^{-11} \text{ Mpc}^{-3}$.

We note that Thompson & Nagamine (2012) computed a number density, but to do so they needed to extrapolate their cumulative v_{12} distribution out to 3000 km s^{-1} owing to their limited volume of $(2.8 \text{ Gpc})^3$. They calculated a value of $n_{\text{FOF}} = 9.4 \times 10^{-13} \text{ Mpc}^{-3}$ for such halo pairs. The use of a larger volume and a better fitting function results in significantly higher values for FOF, and RS additionally provides a number density increase by more than a factor of 30.

Again the distinction must be made that the above values of n represent the number density of *high- v_{12}* halo pairs matching the velocity cut of MB08. Within our largest volume simulation we find 0 FOF pairs, and 35 RS pairs that meet our *massive, high- v_{12}* criteria. We find the number density of *massive, high- v_{12}* halo pairs to be $n_{\text{RS}, \text{massive}} = 1.52 \times 10^{-10}$, i.e. an order of magnitude less than the number density of *high- v_{12}* pairs (n_{RS}).

Using the velocity criteria set by LF14 we find 15 FOF pairs and 535 RS pairs with $d_{12} \leq 10 \text{ Mpc}$, $M_1, M_2 \geq 10^{14} M_\odot$ within our largest simulation. The number densities of these *high- v_{12}* halo pairs is $n_{\text{RS}}(\geq 2799 \text{ km s}^{-1}) =$

$2.04 \times 10^{-9} \text{ Mpc}^{-3}$ and $n_{\text{FOF}}(\geq 2799 \text{ km s}^{-1}) = 7.41 \times 10^{-11} \text{ Mpc}^{-3}$. Again we impose an additional mass cut from LF14 to select *massive, high- v_{12}* candidates and find a number density of $n_{\text{RS}, \text{massive}}(\geq 2799 \text{ km s}^{-1}) = 7.92 \times 10^{-11} \text{ Mpc}^{-3}$. Table 2 summarizes these results.

4.5 Bullet-like pair candidates

We now study in more detail the properties of *massive, high- v_{12}* pairs in the simulation. *Massive, high- v_{12}* pairs are selected from our largest simulation according to the MB08 criteria: (i) $M_1, M_2 \geq 10^{14} M_\odot$, (ii) $\langle M_{12} \rangle \geq 4.14 \times 10^{14} M_\odot$, (iii) $d_{12} \leq 10 \text{ Mpc}$ and (iv) $v_{12} \geq 3000 \text{ km s}^{-1}$. As mentioned in Section 4.4 we find 35 candidates within the RS groupings that meet this criteria, and zero within the FOF groupings.

We select three ideal Bullet-like candidate pairs from the RS *massive, high- v_{12}* sample that best match the Bullet Cluster mass ratio and separation distance, and examine FOF data for the same haloes. The results are summarized in Table 3. RS Bullet-like candidates #1 and #2 are each grouped into a single FOF halo. Pair three however, is identified as two separate FOF groups, but with a v_{12} that is less than half of its RS counterpart (and hence fails to meet the *massive, high- v_{12}* criteria). We note that we used $b = 0.15$ to group FOF haloes; if we had used the canonical value of $b = 0.20$, FOF identifies system #3 as a single group.

By visualizing these systems we can better understand the differences between RS and FOF. In Figure 6 we project the halo particles of our candidate groups onto the $x - y$ plane, and then bin them into hexagonal bins^{3, 4}. The number of FOF-identified particles within a given bin is indicated by the shade of each hexagon, with darker shades corresponding to more particles contained within. Additionally, we indicate the mean velocity vectors of particles within each bin by the colored arrows.

Panels (1) & (2) show halo candidate pairs #1 and #2 from Table 3. Both of these pairs are identified as a single group by FOF; one can clearly see the ‘bridge’ of particles connecting the two concentrations. Arrows indicate the mean velocity of the RS-identified particles within a given bin minus the bulk velocity of the corresponding (single) FOF halo. The directions and magnitudes of the different RS groupings provides clear evidence that the single object identified by FOF is indeed two separate objects when viewed in velocity space. We do not show FOF velocity information, but it is very similar to that of RS since the actual particles grouped into RS and FOF haloes are quite similar; the difference is that, by using velocity information, RS is able to separate these systems into two distinct haloes whereas FOF (which does not use velocity information) lumps them into one.

Candidate #3 is distinct since both FOF and RS identify them as two separate haloes. Here we only show the smaller ‘bullet’ from this pair in Panel (3) of Figure 6, since the larger halo is identified similarly by both. We

³ Interactive 3D visualizations are available at <http://www.physics.unlv.edu/~rthompson/bulletCandidates>

⁴ Hexagonal bins are the closest one can get to a circle while still allowing the shapes to interlock. This makes a hexagonal tessellation the most efficient and compact division of 2D data.

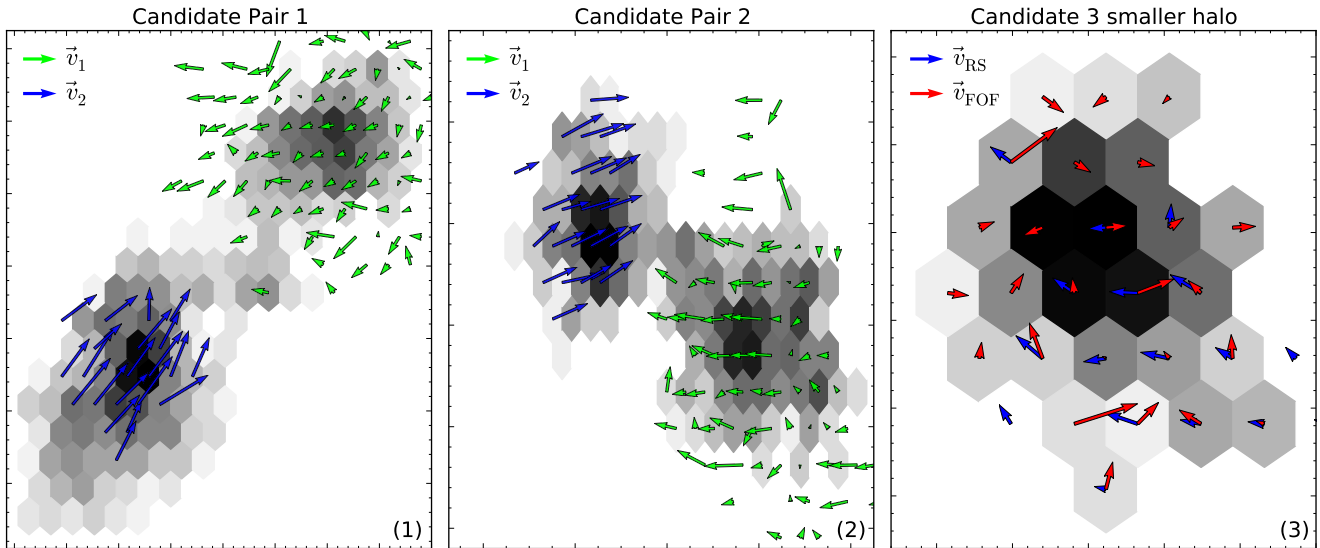


Figure 6. Candidate halo pairs from Table 3 projected on the $x - y$ plane. Greyscale intensity represents the number of FOF identified particles contained within each hexagonal bin. The size of each bin corresponds roughly to the FOF linking length of $\simeq 0.4\text{Mpc}$ ($b = 0.15$). Panels (1) & (2) show RS-identified mean particle velocity vectors from each bin. To accentuate the differences we also subtract the FOF halo’s bulk velocity from the RS velocities. In these cases, FOF groups the two concentrations into a single halo, whereas RS separates them into two haloes based on their distinct kinematics. Panel (3) only shows the smaller halo from candidate pair #3; here we also overplot the FOF velocity vectors in red. Where most of the particles lie (the dark region), the velocity vectors of RS and FOF are in the opposite direction, showing that again FOF is merging kinematically distinct components that RS separates. The resulting pairwise velocity relative to the main halo (not shown) is much smaller in the FOF case.

further show the median velocity vectors for both FOF-identified particles (red) and RS-identified particles (blue). While some bins have similar mean velocities, others are considerably different from one another. Most notably, two of the dark center bins where the majority of the mass lies show nearly opposing velocity vectors between FOF and RS. What has happened is that there are multiple objects in this region, and FOF has overgrouped them resulting in a velocity much closer to that of the main halo (not shown). Meanwhile, RS is able to distinguish the relatively small ‘bullet’ that is distinct in velocity space. The overgrouping results in an FOF halo that is $7\times$ more massive than the RS counterpart, and double in radius. Crucially, the pairwise velocity is reduced by a factor of two when compared to the RS results.

By lumping together multiple groups into a single object, the overall bulk velocity can easily get washed out. Consider this simple example: two head-on merging haloes are grouped together; their bulk velocities would effectively cancel out leading to a much lower bulk velocity for the final group. When v_{12} is calculated between this group and others, the resulting value would be much lower than if they were considered as separate objects. This problem is exacerbated as the number of distinct objects grouped together increases. Candidate #3 is one clear example of such a process.

5 CONCLUSIONS

In this work we determine the probability and number density of finding systems analogous to progenitors of the Bullet Cluster 1E0657-56 within large-volume cosmological N-

body simulations. We particularly examine the difference between two popular halo finding algorithms in the context of searching for a massive, high-pairwise velocity halo pair. Our results show that halo finders that only consider particle positions (FOF) can underestimate the probability of high pairwise velocity systems, which can ultimately lead to tension with the ΛCDM model. Halo finders that additionally consider particle velocities can more robustly identify kinematically distinct substructures, resulting in greater v_{12} probabilities, alleviating tensions with ΛCDM .

Within our largest cosmological N-body simulation, we find the probability of producing a halo pair with $v_{12} \geq 3000\text{ km s}^{-1}$ (Mastropietro & Burkert 2008) from among all halo pairs with $d_{12} \leq 10\text{Mpc}$, & $M_1, M_2 \geq 10^{14} M_\odot$ to be $P_{\text{RS}} = 4.58 \times 10^{-4}$ when using ROCKSTAR (RS). This value is larger by 1.5 dex than when one only considers particle positions using a friends-of-friends (FOF) halo finding algorithm ($P_{\text{FOF}} = 1.35 \times 10^{-5}$). Simulation box size still plays an important role as we show in Figure 2, but using RS, a box size on the order of $(3\text{Gpc})^3$ yields similar probabilities as a $(6.4\text{Gpc})^3$ box with reasonable extrapolations of the v_{12} probability distribution functions. If we slide the velocity cut back to $v_{12} \geq 2799\text{ km s}^{-1}$ as argued by Lage & Farrar (2014a) we find slightly higher probabilities of $P_{\text{RS}}(\geq 2799\text{ km s}^{-1}) = 7.57 \times 10^{-4}$ and $P_{\text{FOF}}(\geq 2799\text{ km s}^{-1}) = 2.89 \times 10^{-5}$. We also find that these results do not change drastically when fitting with “Extreme Value Statistics” rather than a skewed Gaussian.

We estimate the expected number density of such *high- v_{12}* objects to be $n_{\text{RS}} = 1.23 \times 10^{-9}\text{ Mpc}^{-3}$ using the velocity cuts of MB08, and $n_{\text{RS}}(\geq 2799\text{ km s}^{-1}) = 2.04 \times 10^{-9}\text{ Mpc}^{-3}$ for LF14. Imposing an additional mass criteria of

$\langle M_{12} \rangle \geq 4.14 \times 10^{14} M_{\odot}$ (MB08) in order to identify more massive systems that are truer analogs of the Bullet Cluster, we calculate the expected number density of *massive, high- v_{12}* objects to be $n_{\text{RS}, \text{massive}} = 1.52 \times 10^{-10} \text{ Mpc}^{-3}$. Including this more stringent mass criterion, RS identifies $\simeq 35$ *massive, high- v_{12}* candidates within our largest simulation, wherein FOF applied to the same simulation identifies none. Imposing higher mass cut of $\langle M_{12} \rangle \geq 1.08 \times 10^{15} M_{\odot}$ (LF14) yields a number density of *massive, high- v_{12}* objects to be slightly smaller ($n_{\text{RS}, \text{massive}}(\geq 2799 \text{ km s}^{-1}) = 7.92 \times 10^{-11} \text{ Mpc}^{-3}$).

By studying individual examples, we show that the differences between RS and FOF owe to the identification of more substructure by considering particle velocities. We identify three ideal candidate halo pairs from the RS dataset and examine the FOF data in the same region (Table 3). By not considering particle velocities, FOF tends to over-group haloes and/or group together particles that are clearly different groups in velocity space (Figure 6).

We do not expect to find an exact match to the Bullet Cluster within one random realization of our Universe. The more significant point is that producing such *massive high- v_{12}* pairs should no longer be considered a challenge to Λ CDM, as was suggested in Lee & Komatsu (2010) and Thompson & Nagamine (2012). As we have shown here, the identification of such a pair is not only possible but likely when a kinematic halo finding algorithm is used. While for the overall halo population the differences between RS and FOF are fairly minor, using particle velocity information is crucial when identifying haloes in the context of this particular problem.

More broadly, this greatly ameliorates a major challenge to the Λ CDM model presented by the high progenitor pairwise velocities of the Bullet Cluster. Instead, we show that the Bullet Cluster is a rare but expected object in a Λ CDM universe. Future all-sky X-ray surveys (e.g., eROSITA⁵) together with upcoming weak lensing surveys (e.g., LSST⁶) will potentially identify many more Bullet-like systems to lower masses and/or higher redshifts, which can be used to further explore the nature of dark matter, and thus test the Λ CDM paradigm in more detail. At this time, however, the Bullet Cluster provides unequivocal support for the modern concordance cosmological paradigm.

ACKNOWLEDGEMENTS

We thank the anonymous referee for their helpful comments. The simulations used in this paper were run on ‘Blue Waters’ at the National Center for Supercomputing Applications (NCSA), and the data was analyzed on the ‘Timon’ cluster at the University of the Western Cape with pyGadgetReader⁷ (Thompson 2014) & SPHGR⁸ (Thompson 2015). This research is part of the Blue Waters sustained-petascale computing project, which is supported by the National Science Foundation (awards OCI-0725070 and ACI-1238993) and the state of Illinois. Blue Waters is a joint effort of the

University of Illinois at Urbana-Champaign and NCSA. This work is also part of the PRAC allocation, supported by the National Science Foundation (award number OCI-0832614). Support for this work was provided by the South African Research Chairs Initiative and the South African National Research Foundation, along with NASA grant NNX12AH86G. KN is grateful to the discussion with Dr. Tomoaki Ishiyama on large N-body simulations.

REFERENCES

- Behroozi, P. S., Wechsler, R. H., & Wu, H.-Y. 2013, *ApJ*, 762, 109
- Bouillot, V. R., Alimi, J.-M., Corasaniti, P.-S., & Rasera, Y. 2014, *ArXiv e-prints*:1405.6679B
- Bradač, M., Clowe, D., Gonzalez, A. H., Marshall, P., Forman, W., Jones, C., Markevitch, M., Randall, S., Schrabback, T., & Zaritsky, D. 2006, *ApJ*, 652, 937
- Clowe, D., Bradač, M., Gonzalez, A. H., Markevitch, M., Randall, S. W., Jones, C., & Zaritsky, D. 2006, *ApJL*, 648, L109
- Clowe, D., Gonzalez, A., & Markevitch, M. 2004, *ApJ*, 604, 596
- Courtin, J., Rasera, Y., Alimi, J.-M., Corasaniti, P.-S., Boucher, V., & Füzfa, A. 2011, *MNRAS*, 410, 1911
- Davis, M., Efstathiou, G., Frenk, C. S., & White, S. D. M. 1985, *ApJ*, 292, 371
- Fisher, R. A. & Tippet, L. H. C. 1928, *Proc. Cambridge Philosophical Soc.*, 24, 180
- Frechet, M. 1927, *Ann. Soc. Polon. Math.*, 6, 93
- Gnedenko, V. 1943, *Annals of Mathematics*, 44, 423
- Gumbel, E. J. 1935, *Ann. Inst. Henri Poincaré*, 5, 115
- Hayashi, E. & White, S. D. M. 2006, *MNRAS*, 370, L38
- Hinshaw, G., Larson, D., Komatsu, E., Spergel, D. N., Bennett, C. L., Dunkley, J., Nolte, M. R., Halpern, M., Hill, et al. 2013, *ApJS*, 208, 19
- Jenkins, A., Frenk, C. S., White, S. D. M., Colberg, J. M., Cole, S., Evrard, A. E., Couchman, H. M. P., & Yoshida, N. 2001, *MNRAS*, 321, 372
- Knebe, A., Knollmann, S. R., Muldrew, S. I., Pearce, F. R., Aragon-Calvo, M. A., Ascasibar, Y., Behroozi, P. S., Ceverino, & others. 2011, *MNRAS*, 415, 2293
- Lage, C. & Farrar, F. 2014a, *ArXiv e-prints*:1406.6703
- Lage, C. & Farrar, G. 2014b, *ApJ*, 787, 144
- Lee, J. & Komatsu, E. 2010, *ApJ*, 718, 60
- Markevitch, M. 2006, in *ESA Special Publication*, Vol. 604, The X-ray Universe 2005, ed. A. Wilson, 723–+
- Mastropietro, C. & Burkert, A. 2008, *MNRAS*, 389, 967
- Milosavljević, M., Koda, J., Nagai, D., Nakar, E., & Shapiro, P. R. 2007, *ApJL*, 661, L131
- More, S., Kravtsov, A. V., Dalal, N., & Gottlöber, S. 2011, *ApJS*, 195, 4
- Planck Collaboration, Ade, P. A. R., Aghanim, N., Armitage-Caplan, C., Arnaud, M., Ashdown, M., Atrio-Barandela, F., Aumont, J., Baccigalupi, C., Banday, A. J., & et al. 2013, *ArXiv e-prints*:1303.5076
- Robertson, B. E., Kravtsov, A. V., Tinker, J., & Zentner, A. R. 2009, *ApJ*, 696, 636
- Sheth, R. K. & Tormen, G. 1999, *MNRAS*, 308, 119
- Springel, V. 2005, *MNRAS*, 364, 1105
- Springel, V. & Farrar, G. R. 2007, *MNRAS*, 380, 911

⁵ <http://www.mpe.mpg.de/eROSITA>

⁶ <http://www.lsst.org/lsst>

⁷ <https://bitbucket.org/rthompson/pygadgetreader>

⁸ <https://bitbucket.org/rthompson/sphgr>

- Springel, V., White, S. D. M., Tormen, G., & Kauffmann, G. 2001, MNRAS, 328, 726
- Thompson, R. 2014, pyGadgetReader: GADGET snapshot reader for python, Astrophysics Source Code Library:1411.001
- . 2015, SPHGR: Smoothed-Particle Hydrodynamics Galaxy Reduction, Astrophysics Source Code Library:1502.012
- Thompson, R. & Nagamine, K. 2012, MNRAS, 419, 3560
- Tinker, J., Kravtsov, A. V., Klypin, A., Abazajian, K., Warren, M., Yepes, G., Gottlöber, S., & Holz, D. E. 2008, ApJ, 688, 709
- Watson, W. A., Iliev, I. T., Diego, J. M., Gottlöber, S., Knebe, A., Martínez-González, E., & Yepes, G. 2014, MNRAS, 437, 3776

Table 2. Probabilities & number densities

Pairs	N _{RS}	N _{FOF}	P _{RS}	P _{FOF}	n _{RS}	n _{FOF}
Mastropietro & Burkert (2008) criteria						
<i>High-v</i> ₁₂	318	6	4.58×10^{-4}	1.35×10^{-5}	1.23×10^{-9}	3.45×10^{-11}
<i>Massive, high-v</i> ₁₂	35	0	1.36×10^{-3}	7.38×10^{-6}	1.52×10^{-10}	-
Lage & Farrar (2014a) criteria						
<i>High-v</i> ₁₂	535	15	7.57×10^{-4}	2.89×10^{-5}	2.04×10^{-9}	7.41×10^{-11}
<i>Massive, high-v</i> ₁₂	23	0	5.84×10^{-2}	9.41×10^{-6}	7.92×10^{-11}	-

Note. — *High-v*₁₂ pairs are defined as halo pairs with $v_{12} \geq 3000 \text{ km s}^{-1}$ (MB08), or $v_{12} \geq 2799 \text{ km s}^{-1}$ (LF14) from among all halo pairs with $M_1, M_2 \geq 10^{14} M_\odot$ and $d_{12} \leq 10 \text{ Mpc}$. *Massive, high-v*₁₂ pairs are defined by imposing an additional mass criteria of $\langle M_{12} \rangle \geq 4.14 \times 10^{14} M_\odot$ (MB08) or $\langle M_{12} \rangle \geq 1.08 \times 10^{15} M_\odot$ (LF14). All values are from our largest volume simulation. ‘N’ is the total number of pairs that meet said criteria, ‘P’ represents the probability (Section 4.3), and ‘n’ is the number density given in units of Mpc^{-3} . Previous works found $P_{\text{FOF}} = 6.4 \times 10^{-6}$ (Bouillot et al. 2014), and $n_{\text{FOF}} = 9.4 \times 10^{-13}$ (Thompson & Nagamine 2012) for *high-v*₁₂ pairs when imposing the MB08 velocity cut.

Table 3. Bullet-like candidate pairs

Pair	v_{12} [km s ⁻¹]	d_{12} [Mpc]	θ	M_1 [M_\odot]	M_2 [M_\odot]	Mass Ratio	r_1 [Mpc]	r_2 [Mpc]
Rockstar Candidates								
1	4893	5.95	156	1.69e15	2.01e14	0.08	2.34	1.00
2	3506	3.57	149	1.65e15	2.06e14	0.13	2.32	1.16
3	3130	6.17	141	1.88e15	1.30e14	0.07	2.42	0.99
FOF Findings								
1	Single	-	-	4.19e15	-	-	3.17	-
2	Single	-	-	2.48e15	-	-	2.66	-
3	1537	5.69	131	1.56e15	9.21e14	0.59	2.28	1.91

Note. — Selected *massive, high-v*₁₂ candidate pairs from our largest simulation (see Table 1). Rockstar candidates were chosen based on how similar they were to the Bullet Cluster initial condition requirements of Mastropietro & Burkert (2008). Corresponding FOF haloes were then identified based on their proximity to the chosen RS haloes.